Yuan, Y. & Whittle, A. J. *Géotechnique* [https://doi.org/10.1680/jgeot.16.P.276]

A novel elasto-viscoplastic formulation for compression behaviour of clays

Y. YUAN* and A. J. WHITTLE†

This paper presents a novel elasto-viscoplastic formulation for describing the time-dependent compression behaviour of clays. The formulation incorporates a novel flow rule that attributes viscoplastic strain rate to an internal state variable representing the perturbation of the clay particle assembly due to historical straining. The proposed model can describe a wide range of observed time effects under constant rate of strain loading conditions, including both isotache and temporary effects of step changes in strain rate, while allowing creep and relaxation by way of an auto-decay process of internal strain rate. The model facilitates rational estimates of the initial creep rate in the analyses of consolidation for thick clay layers (field scale) and, hence, overcomes drawbacks of existing isotache models. The proposed formulation is also able to represent diverse observations of primary consolidation for clay layers of different thicknesses, providing a unifying framework that can resolve the long-standing paradox in observed clay behaviour (hypotheses A and B). The model is applied to re-interpret the effects of specimen thickness on the consolidation behaviour of Osaka Bay mud in laboratory tests and show that apparent contradictions in the data can be related to rate-dependent properties of the clay.

KEYWORDS: clays; consolidation; constitutive relations; creep; plasticity; time dependence

INTRODUCTION

The compressibility of saturated clays is of great importance in many practical geotechnical problems, especially those demanding accurate predictions of long-term settlements. Building on the concept of effective stress (Terzaghi, 1943) it is long-established practice to model the one-dimensional (1D) 'primary' consolidation process (coupled flow and deformation) following assumptions that: (*a*) seepage of the pore fluid is controlled by Darcy's law, where the hydraulic conductivity, k, is a monotonic function of the void ratio, e; and (*b*) non-linear compression of the soil skeleton is represented by elastoplastic stiffness properties that vary with stress history but are independent of time. The compression behaviour of normally consolidated (NC) clay is typically linearised by a virgin consolidation line (VCL) in e–log σ'_v space (Terzaghi & Peck, 1948; Schofield & Wroth, 1968), which defines density hardening within elastoplastic models. Several authors have highlighted limitations of the conventional e–log σ'_v framework both in representing the non-linear compression of natural clays (Juarez-Badillo, 1965; Butterfield, 1979) and in imposing unrealistic constraints on tangent stiffness properties (Janbu, 1963; Pestana & Whittle, 1999). The current work builds on the framework proposed by Pestana & Whittle (1999), which linearises clay compression behaviour in log e–log σ'_v space (and compression properties of NC clays are represented by a limiting compression curve (LCC), Fig. 1). This framework has advantages over the conventional e–log σ'_v space, as the former provides a more realistic model of the 1D modulus, M (i.e. $\partial M/\partial e < 0$) and can more effectively linearise the compression behaviour of natural clays (Pestana, 1994).

The assumption of time-independent compression behaviour neglects a long-recognised fact that clays inherently exhibit viscous characteristics, which are generally attributed to viscous physico-chemical interactions occurring at the micro-scale (Le *et al*., 2012). These viscous characteristics are evident in observations of creep (Buisman, 1936), strain rate effects (Leroueil *et al*., 1985) and relaxation (Yoshikuni *et al*., 1995) at the laboratory scale. Viscous properties of clays also impact the prediction of primary consolidation (Taylor, 1942; Bjerrum, 1967; Leroueil *et al*., 1985; Mesri & Choi, 1985b; Imai, 1995). Therefore, using time-dependent constitutive laws not only enables more realistic representations of deformation mechanisms for clays, but is also important for achieving more reliable predictions of long-term field consolidation.

Numerous elasto-viscoplastic (EVP) frameworks have been proposed for time-dependent behaviour of clays (after Perzyna, 1966), but few of them have been widely used in practice. The greatest challenge in developing EVP frameworks lies in the assumption of the spontaneous development of viscoplastic strain. In the literature, the isotache (Suklje, 1957) or equivalent isochrone (Bjerrum, 1967) frameworks have become a popular basis for many models (e.g., Garlanger, 1972; Yin & Graham, 1994; Den Haan, 1996; Vermeer & Neher, 1999; Kim & Leroueil, 2001; Yin *et al*., 2010; Bodas Freitas *et al*., 2011), which typically assume a power-law equation for the viscoplastic (creep) strain rate

$$\dot{\varepsilon}^{vp} = \dot{\varepsilon}_{ref}\left(\frac{\sigma'_v}{\sigma'_p}\right)^{\alpha} \tag{1}$$

where $\dot{\varepsilon}_{ref}$ is a material constant representing reference strain rate, often obtained as strain rate at the end of a 24 h interval in an incrementally loaded (IL) oedometer test ($\approx 3{\cdot}6 \times 10^{-2}$%/h); σ'_p acts as a yield stress that depends on

Manuscript received 29 October 2016; revised manuscript accepted 19 January 2018.
Discussion on this paper is welcomed by the editor.
* GZA GeoEnvironmental Inc., Norwood, MA, USA; Formerly Massachusetts Institute of Technology, Cambridge, MA, USA (Orcid:0000-0002-3408-0358).
† Edmund K. Turner Professor of Civil & Environmental Engineering, Massachusetts Institute of Technology, Cambridge, MA, 02139, USA.

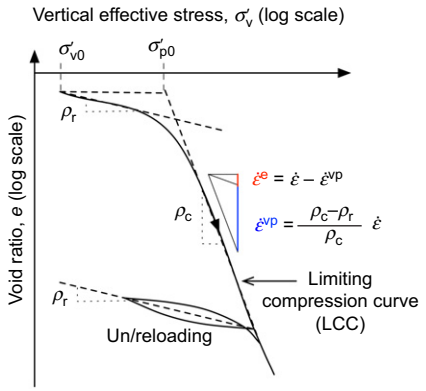

Fig. 1. Schematic illustration of log$e$–log σ'_v framework for compression behaviour of clay (after Pestana, 1994)

void ratio, e, while the stress ratio σ'_p/σ'_v is defined by the stress history. The exponent, α, represents the rate-sensitivity of the constitutive relation, which is often linked to the ratio between virgin compression index and conventional secondary compression, C_c/C_α (Mesri & Castro, 1987).

The underlying assumption of the isotache formulation is that viscoplastic strain rate, $\dot{\varepsilon}^{vp}$, can be uniquely defined by the current states of σ'_v and e. However, this empirical assumption can lead to limitations when predicting consolidation behaviour at field scale. For instance, isotache models tend to overestimate the initial viscoplastic rate, $\dot{\varepsilon}^{vp}$, for the consolidation of thick clay layers: for an NC clay (i.e. $\sigma'_p/\sigma'_v \approx 1{\cdot}0$), equation (1) with $\dot{\varepsilon}_{ref} \approx 3{\cdot}6 \times 10^{-2}$%/h obtained at laboratory scale will predict an initial creep rate, $\dot{\varepsilon}^{vp} \approx 3{\cdot}6 \times 10^{-2}$%/h (≈1 %/day) for the soil at field scale (at the same σ'_v and e as used in the laboratory test). Such a high creep rate is likely to exceed the typical strain rate implied by pore pressure dissipation in field-scale consolidation (Yuan & Whittle, 2013). Adjustment in the state parameters, σ'_p or e, is then needed to improve predictions at field scale. This approach is often justified by invoking effects of sample disturbance (Degago & Grimstad, 2014).

According to isotache theory the strain at the end of primary (EOP) consolidation increases with the thickness of the clay, but generates unique secondary compression behaviour. This type of behaviour conforms to hypothesis B behaviour as framed by Ladd *et al.* (1977). However, there are many contradictory data and experiences, which suggest that similar levels of strain can occur at EOP for clay layers of different thickness (e.g. Mesri & Choi, 1985a, 1985b; Watabe *et al.*, 2008), which is often referred to as hypothesis A (Ladd *et al.*, 1977). To date hypothesis A behaviour can only be described either by artificially excluding creep during primary consolidation (Jamiolkowski *et al.*, 1985), or assuming unique stress–strain behaviour at EOP (Mesri & Choi, 1985a). To the authors' knowledge, there is no constitutive model for clays that can represent reliably the full range of thickness effects reported for IL consolidation (i.e. a single framework capable of simulating both hypothesis A and B).

This paper presents a new EVP framework for one-dimensional (1D) time-dependent compression behaviour of clay. The proposed model uses a novel evolution law that attributes the viscoplastic strain rate to an internal state variable, which represents the perturbation of the clay particle assembly through the past history of straining (i.e. strain rate history). The concept can be related to the granular temperature in the theoretical framework of granular thermodynamics (Smith, 2001) or granular solid hydrodynamics (Jiang & Liu, 2009, 2013; Zhang & Chen, 2014). Its extension in the present EVP formulation describes a broad range of time-dependent characteristics of clays, and overcomes the drawbacks of existing isochrone- or isotache-based models.

FORMULATION OF PROPOSED MODEL

The proposed formulation assumes that the total strain rate is a superposition of elastic and viscoplastic components.

$$\dot{\varepsilon} = \dot{\varepsilon}^e + \dot{\varepsilon}^{vp} \tag{2}$$

This relation is defined in the log$e$–log σ' space following Pestana (1994), as shown in Fig. 1. The elastic unloading/reloading curve is linearised with a constant slope, ρ_r (an extended formulation with a variable ρ_r is also available in the thesis by Yuan (2016)), while the LCC has a constant slope, ρ_c. These compressibility parameters can be related to the conventional recompression and virgin compression indices ($\rho_r = 0{\cdot}434C_r/e$ and $\rho_c = 0{\cdot}434C_c/e$), while the elastic strain rate, $\dot{\varepsilon}^e$, can be readily evaluated in terms of the changes in effective stress, $\dot{\sigma}'_v/\sigma'_v$, porosity, n, and ρ_r

$$\dot{\varepsilon}^e = \rho_r n \frac{\dot{\sigma}'_v}{\sigma'_v} \tag{3}$$

Viscoplastic flow rule

Equation (4) defines viscoplastic strain rate as a product of a new state variable, R_a, with units of strain rate (1/time), and a stress ratio, σ'_v/σ'_p.

$$\dot{\varepsilon}^{vp} = R_a \left(\frac{\sigma'_v}{\sigma'_p}\right) \tag{4}$$

where R_a (≥ 0) is a new state variable, representing an internal strain rate corresponding to the overall perturbation of the clay particle assembly.

The value of σ'_p is a reference stress state defined on the LCC (Fig. 1), and is subject to density hardening during compression (equation (5)).

$$\frac{\dot{\sigma}'_p}{\sigma'_p} = \frac{\dot{\varepsilon}}{\rho_c n} = \frac{\dot{\varepsilon}^{vp}}{(\rho_c - \rho_r)n} \tag{5}$$

The internal strain rate, R_a, can be equated with the thermodynamic concept of granular temperature, which describes the kinetic energy level (associated with random motions of particles) within a granular assembly that is perturbed from an equilibrium state (after Smith, 2001; Shattuck *et al.*, 2009; Jiang & Liu, 2009, 2013). Although there are currently no direct measurements of kinetic energy for clay particles, the framework logically explains processes of creep or relaxation after the cessation of prior loading or straining events. The framework is also broadly consistent with Taylor's qualitative description, which associates secondary compression with 'the disturbance and remolding effects caused by primary consolidation' (Taylor, 1942: pp. 52–53).

The proposed description of viscoplastic strain rate (equation (4)) is distinct from the unique σ'_v–ε–$\dot{\varepsilon}^{vp}$ relationship assumed by prior isochrone or isotache theories, where the creep rate is only a function of current states. As demonstrated later, by accommodating historical straining effects, the proposed model allows a more versatile description of creep behaviour with great implications for predictions of long-term consolidation.

The temporal evolution of the internal strain rate is based on an activation and decay mechanism

$$\dot{R}_a = [f(\dot{\varepsilon}) - R_a]m_t \tag{6}$$

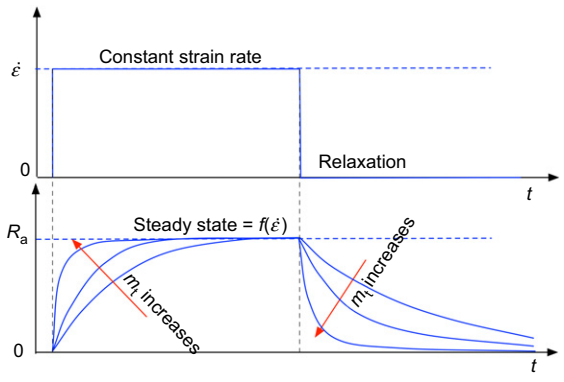

Fig. 2. Influence of m_t on the evolution of R_a during CRS compression and relaxation

Equation (6) shows that the internal strain rate, R_a, increases with an activation function of the total strain rate, $f(\dot{\varepsilon})$, representing the effects of mechanical stimulation (e.g. external straining) on the soil skeleton. Simultaneously, there is an auto-decay process controlled by the current value of the internal strain rate ($-R_a$) as the clay particles adjust towards a new equilibrium state after perturbation. The net change is then scaled by a transient coefficient, m_t, with units (1/time).

Figure 2 illustrates schematically how the transient coefficient, m_t, influences the evolution of R_a for compression at constant rate of strain (CRS; at prescribed $\dot{\varepsilon}$) and a succeeding relaxation phase ($\dot{\varepsilon} = 0$). There is a transient response in the internal strain rate, R_a, due to the initial step change in external strain rate, converging to a steady-state condition that is a function of the applied strain rate, $f(\dot{\varepsilon})$. The steady-state condition closely pertains to the normal consolidation behaviour of clay in a CRS consolidation test. During relaxation, R_a decreases towards zero as time elapses. As can be seen, the changing rate of R_a increases with m_t for both the transient increase and decay processes. In the extreme case, a very large value of m_t leads to almost instantaneous change in R_a with $\dot{\varepsilon}$ (as a result, the development of irrecoverable deformation, i.e. controlled by R_a in equation (4), becomes time independent). In order to achieve more realistic descriptions of time-dependent behaviour of clay, the proposed model requires definitions for the activation function, $f(\dot{\varepsilon})$, and transient coefficient, m_t, as follows.

Activation function

Under CRS conditions, equation (6) allows a transient change in R_a towards a steady state, $f(\dot{\varepsilon})$. The function $f(\dot{\varepsilon})$ can be defined for matching the normal consolidation characteristics in CRS tests as follows.

$$f(\dot{\varepsilon}) = \left(\frac{\rho_c - \rho_r}{\rho_c}\dot{\varepsilon}\right)\left(\frac{\dot{\varepsilon}}{\dot{\varepsilon}_{ref}}\right)^{-\beta} \tag{7}$$

The first term, $[(\rho_c - \rho_r)/\rho_c]\dot{\varepsilon}$, is equal to the viscoplastic strain rate for compression along an LCC line, as illustrated in Fig. 1. The power-law function allows $f(\dot{\varepsilon})$ to be rate-dependent, where $\dot{\varepsilon}_{ref}$ represents a reference strain rate, and the exponent $(-\beta)$ controls the rate-sensitivity of $f(\dot{\varepsilon})$. By varying β, the proposed formulation can describe a wide range of rate-dependent characteristics observed in CRS tests. Under CRS conditions, as R_a reaches the steady-state function, $f(\dot{\varepsilon})$, the flow rule of equation (4) becomes

$$\dot{\varepsilon}^{vp} = \frac{\rho_c - \rho_r}{\rho_c}\dot{\varepsilon}\left(\frac{\dot{\varepsilon}}{\dot{\varepsilon}_{ref}}\right)^{-\beta}\left(\frac{\sigma'_v}{\sigma'_p}\right) \tag{8}$$

For compression in the LCC region, that is, $\dot{\varepsilon}^{vp} = [(\rho_c - \rho_r)/\rho_c]\dot{\varepsilon}$, equation (8) with $\beta = \rho_\alpha/\rho_c$ matches the power-law isotache formulation (equation (1)). In this case, the proposed model describes parallel LCC lines for CRS tests, with each corresponding to a specific strain rate, Fig. 3(a). The faster strain rate generates higher effective stress levels at the same void ratio, and LCCs with one log cycle of difference in strain rate have equal spacing. The same value of β can also lead to parallel shifts in the LCC locus for

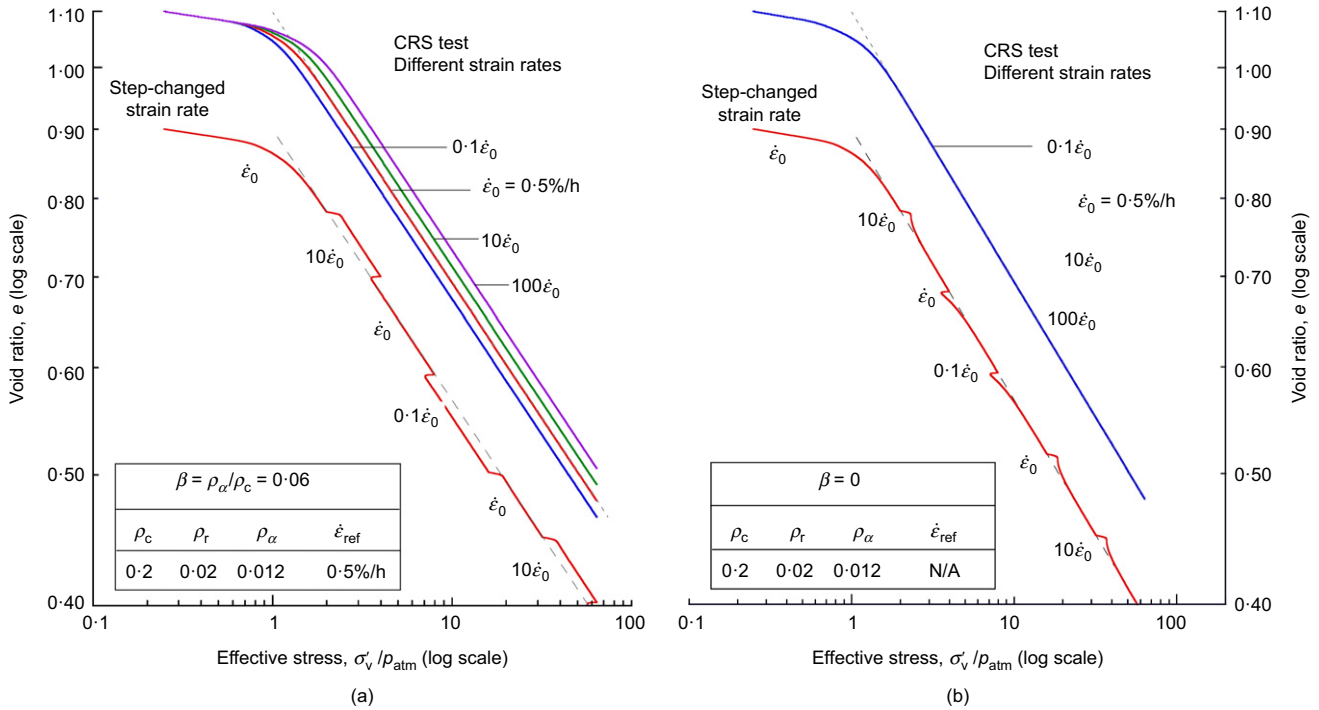

Fig. 3. Demonstration of predicted rate effects on effective stress–void ratio curves for CRS tests: (a) with $\beta = \rho_\alpha/\rho_c$; (b) with $\beta = 0$

a CRS test using stepped changes in strain rates, as also shown in Fig. 3(a). These results are consistent with conventional isotache theory (Suklje, 1957).

On the other hand, if $\beta = 0$ in equation (8), the proposed model conforms to a bounding plasticity formulation (cf. Pestana & Whittle, 1999), where the irrecoverable deformation in an overconsolidated (OC) state is mapped from an NC state using an effective stress ratio (σ'_v/σ'_p). Fig. 3(b) shows that the proposed model predicts a unique LCC independent of the strain rates used in CRS simulations. However, the model predicts transient effects of stepped changes in strain rates in a CRS test, as shown in Fig. 3(b). Each change in strain rate causes an immediate jump in effective stress, but these effects are only temporary and the compression response converges to a unique LCC. This behaviour conforms to the 'temporary effects of strain rate and acceleration' (TESRA) framework proposed by Tatsuoka *et al.* (2002).

The present implementation of the model assumes a constant rate-dependency, β, for simplicity. However, some researchers have reported a variation in rate-dependency with strain rates (Watabe *et al.*, 2012). Although this issue can explain some of the contradictory creep data reported in the literature (and is discussed in the section later in this paper entitled 'Interpretation of data for Osaka Bay mud'), it is beyond the scope of the current model formulation.

Transient coefficient

The transient coefficient, m_t, is of particular importance for describing 'delayed processes' such as secondary compression or relaxation where the activation function $f(\dot{\varepsilon})$ is insignificant and the decay term (equation (6)) dominates. The transient coefficient is assumed to be a function of the viscoplastic strain rate

$$m_t = \left(\frac{\rho_c}{\rho_\alpha} - 1\right)\frac{\dot{\varepsilon}^{vp}}{\rho_r n} + O(\dot{\varepsilon}) \tag{9}$$

where ρ_α is a material constant characterising the creep behaviour of clay, with a similar role to the secondary compression coefficient, C_α. A small contingency term $O(\dot{\varepsilon})$ is introduced to allow m_t to increase for limiting cases when $\dot{\varepsilon}^{vp} = 0$ (and $\dot{\varepsilon} > 0$). This condition is generally achieved by assuming $O(\dot{\varepsilon}) = \dot{\varepsilon}$.

When simulating relaxation, the activation function $f(\dot{\varepsilon}) = 0$, and equation (6) gives $\dot{R}_a/R_a = -m_t$. Then, using equation (9), the decrease in effective stress that is controlled by viscoplastic strain (because $\dot{\varepsilon}^e = -\dot{\varepsilon}^{vp}$ during relaxation), can be attributed to the auto-decay in R_a

$$\frac{\dot{\sigma}'_v}{\sigma'_v} = -\frac{\dot{\varepsilon}^{vp}}{\rho_r n} \approx \frac{1}{\rho_c/\rho_\alpha - 1}\frac{\dot{R}_a}{R_a} \tag{10}$$

The above relation highlights that the proposed formulation can predict relaxation as long as the internal strain rate, $R_a > 0$, and the decrease in stress rate is proportional to the ratio, ρ_α/ρ_c, but independent of the rate-sensitivity parameter, β. Fig. 4(a) illustrates typical predictions of relaxation behaviour, in terms of logarithmic effective stress plotted against logarithmic elapsed time ($\log \sigma'_v/\sigma'_{vc}$–$\log t$) curve, where stress is normalised by consolidation stress prior to relaxation. After a short transition, the proposed model simulates a linearised relation with slope corresponding to ρ_α/ρ_c. This linearised 1D relaxation behaviour of clays is widely observed in experiments (and has also been modelled by Yin *et al.* (2014)). Fig. 4(a) demonstrates that the proposed model with $\rho_\alpha/\rho_c = 0{\cdot}06$ closely matches the typical relaxation data for Batiscan clay ($w_L = 49\%$, $I_P = 27\%$) and Väsby clay ($w_L = 55\%$, $I_P = 32\%$) (Feng, 1991) in the log σ'_v/σ'_{vc}–log$t$ space.

The transient coefficient m_t also enables versatile descriptions of creep behaviour. During creep, clay deforms under a constant effective stress condition, $\dot{\sigma}'_v = 0$, with strain rate, $\dot{\varepsilon} = \dot{\varepsilon}^{vp}$. Hence, $f(\dot{\varepsilon}) = f(\dot{\varepsilon}^{vp})$ and equation (6) becomes

$$\dot{R}_a = [f(\dot{\varepsilon}^{vp}) - R_a]m_t \tag{11}$$

This relation governs the auto-decay process of internal strain rate, R_a, and hence, viscoplastic strain rate, $\dot{\varepsilon}^{vp}$, throughout the creep process, where m_t determines the decrease rate. Fig. 4(b) illustrates the predicted creep curve for clay after consolidation in a CRS test. The model can predict a continuous development of creep for $0 \le \beta \le \rho_\alpha/\rho_c$. At $\beta = \rho_\alpha/\rho_c$ the model eventually predicts a linearised logarithmic void ratio plotted against logarithmic elapsed time (log$e$–log$t$) curve, with the slope corresponding to ρ_α, which can also be expressed as $0{\cdot}434C_\alpha/e$ for this case. As shown above, the parameter ρ_α plays an important role in describing both the creep and relaxation behaviour.

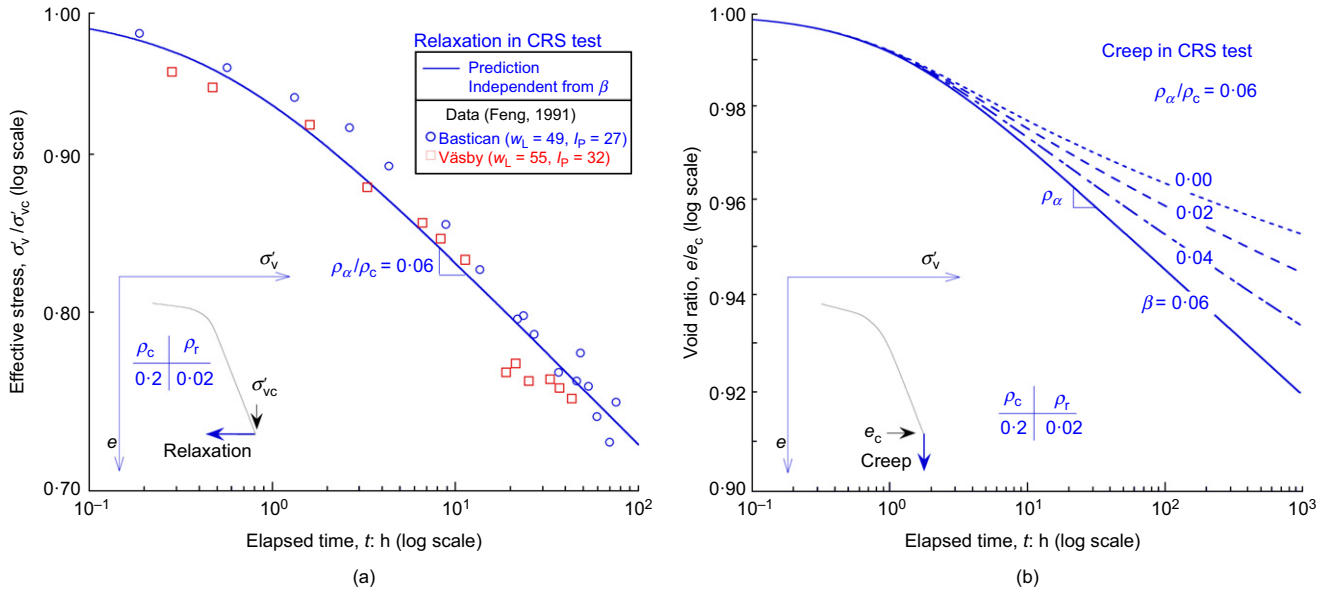

Fig. 4. Demonstration of model predictions for (a) relaxation and (b) creep with different values of β in CRS test

MODEL CALIBRATION

The proposed model introduces five material constants, ρ_r, ρ_c, β, ρ_α and $\dot{\varepsilon}_{ref}$, which can all be determined using experimental data from 1D CRS and IL oedometer tests. The details of the calibration procedure are presented below, with examples using experimental data from CRS tests on San Francisco Bay mud (SFBM, $w_L = 109{\cdot}8\%$, $I_P = 62{\cdot}9\%$) with stepped changes in strain rate (Korchaiyapruk, 2007).

(*a*) Compressibility parameters, ρ_c and ρ_r, can be evaluated directly from the slope of the linearised LCC and unloading/reloading curve, respectively. The data can be obtained from either CRS or IL oedometer tests. Fig. 5 presents data from a CRS test (CRS 691) on SFBM in log$e$–log σ'_v space from which, $\rho_c = 0{\cdot}26$ and $\rho_r = 0{\cdot}0142$ (obtained from the initial recompression curve).

(*b*) The parameter β describes rate-dependency of the steady-state behaviour, and is assumed to be bounded such that $0 \leq \beta \leq \rho_\alpha/\rho_c$. In general, the determination of β can use either multiple CRS tests on the same type of sample at different strain rates, or a single CRS test with a series of step changes in strain rate, such as the considered CRS 691. As shown in Fig. 5, the LCC curve manifests parallel shifts, in terms of changes in effective stress, with the step changes in strain rate between $\dot{\varepsilon} = 0{\cdot}75$, $1{\cdot}5$ and 3%/h. Fig. 6 plots the changes in effective stress against the applied strain rate in a log σ'_v–log$\dot{\varepsilon}$ space for selected void ratios ($e = 2{\cdot}27$–$1{\cdot}70$). The slope of the linear regression at a specific void ratio represents rate-sensitivity, from which a mean value is estimated, $\beta = 0{\cdot}065$. Moreover, the observed rate-dependent LCC for SFBM closely resembles the characteristics of isotache behaviour (cf. Leroueil *et al.*, 1985). This implies a relation for $\rho_\alpha/\rho_c \approx \beta$.

(*c*) In principle, the parameter, ρ_α, can be determined with relaxation or creep data from a CRS or IL oedometer test. During relaxation the ratio ρ_α/ρ_c corresponds to the slope of the linearised log σ'_v–log$t$ curve (cf. Fig. 4(a)), while ρ_α can be obtained through a parametric study to fit the log$e$–log$t$ curve for creep behaviour (cf. Fig. 4(b)). However, the CRS test of SFBM includes neither creep nor relaxation. Considering the above observed isotache characteristics of SFBM, $\rho_\alpha/\rho_c = \beta = 0{\cdot}065$ is assumed in the following computations.

(*d*) The reference strain rate, $\dot{\varepsilon}_{ref}$, only becomes effective for $\beta > 0$. It can be assumed as the applied strain rate in a CRS test, at which the effective stress–void ratio curve is defined as the reference LCC (i.e. where the stress ratio $\sigma'_v/\sigma'_p = 1$). If data for an IL oedometer test are available, $\dot{\varepsilon}_{ref}$ can also be assumed as the average strain rate for a 2 cm thick specimen evaluated at the end of a 24 h interval. Based on the data of the CRS test for SFBM, the reference LCC is chosen at $\dot{\varepsilon}_{ref} = 0{\cdot}75\%$/h.

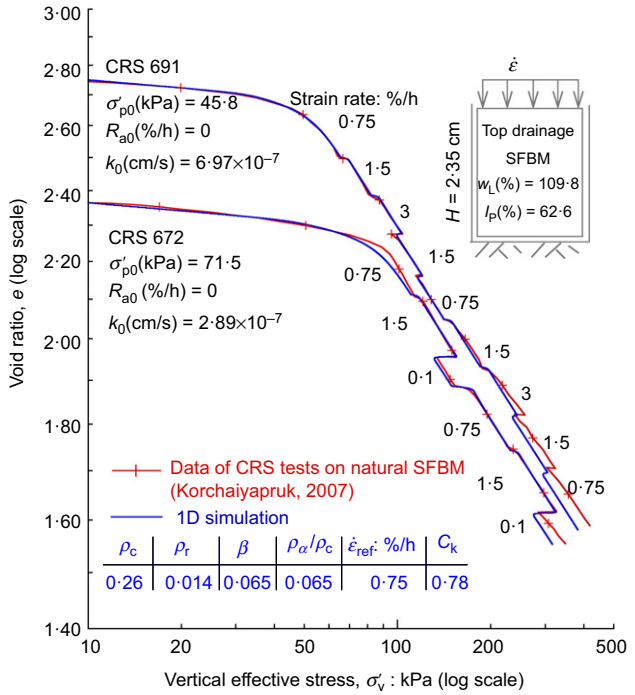

Fig. 5. Comparison between the numerical predictions and experimental results for strain rate effects of SFBM in CRS tests with step-changed strain rates

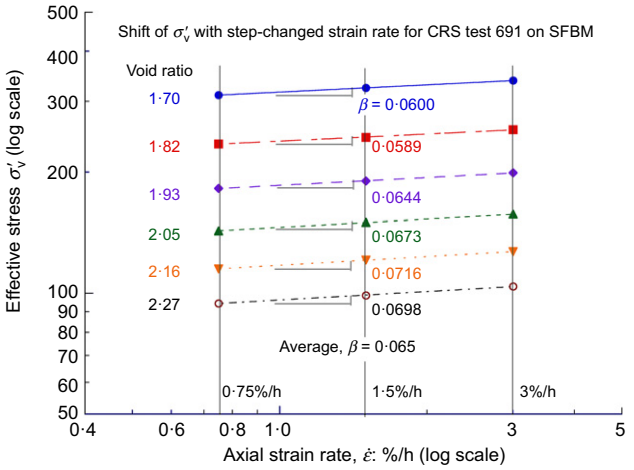

Fig. 6. Determination of rate-sensitivity parameter β from the shift of σ'_v upon step-changed strain rate at different void ratio level

The proposed model also uses two internal state variables: σ'_p to represent stress history effects, and the internal strain rate, R_a, to reflect the effect of strain rate history. The initial values, σ'_{p0} and R_{a0}, can be determined as follows

(*a*) σ'_{p0} can be determined from the compression curve in CRS or IL oedometer tests. The value corresponds to the stress level on the extension of the reference LCC locus at the initial void ratio, e_0. Using the data of CRS 691 on SFBM (Fig. 5), $\sigma'_{p0} = 45{\cdot}8$ kPa for an initial void ratio, $e_0 = 2{\cdot}79$.

(*b*) R_{a0} primarily controls the initial viscoplastic rate in consolidation analyses. For clay initially loaded at an OC state with overconsolidation ratio, OCR > 2, the potential for creep is negligible. This is the case for the current CRS test, and hence, $R_{a0} = 0$. The initial value, R_{a0}, plays an important role in the predictions of consolidation behaviour of NC or slightly OC clay. The next section discusses a method of estimating R_{a0} for NC clay.

With these selected material and state parameters the proposed model is used to reproduce the consolidation behaviour of CRS test 691 for SFBM. Fig. 5 shows good agreement between the predictions and experimental results in terms of the log$e$–log σ'_v response for $e \geq 1{\cdot}9$. The same model parameters are then used to predict a second CRS test (number 672) with step-changed strain rate $\dot{\varepsilon} = 0{\cdot}1$, $0{\cdot}75$ and $1{\cdot}5\%$/h (in this case, $\sigma'_{p0} = 71{\cdot}5$ kPa at $e_0 = 2{\cdot}36$), and results

in good agreement with experimental data. These results demonstrate that the proposed model can describe accurately the rate-dependent characteristics of the SFBM behaviour measured in CRS tests.

KEY FEATURES

Rational estimate of initial creep rate

An important feature of the proposed formulation is that it allows a rational assumption of the initial creep rate for clay layers in consolidation analyses. Unlike isotache formulations, the initial creep rate, $\dot{\varepsilon}_0^{vp}$ (given in equation (4)) is not uniquely defined at the current stress ratio, σ'_p/σ'_v, but also depends closely on the initial value of internal strain rate, R_{a0}. A zero value of R_{a0} is reasonable for clay at $\sigma'_p/\sigma'_v > 2$ (i.e. OC states where there is negligible creep), whereas a realistic estimate of R_{a0} becomes essential for consolidation of NC clay where $\dot{\varepsilon}_0^{vp} \approx R_{a0}$ as $\sigma'_p/\sigma'_v \approx 1$. Although monitoring of ground movements before loading could provide an estimate of $\dot{\varepsilon}_0^{vp}$, such a long-term measurement is rarely available in practice. Herein, a method is proposed to obtain an order of magnitude estimate of creep rate for NC clay.

Assuming the clay layer is consolidated to an average degree of consolidation of 99%, the internal creep rate and total strain rate both reach equilibrium. The average creep rate across the thickness can be estimated from the estimated creep coefficient, ρ_α, as $\dot{\varepsilon}_0^{vp} = \rho_\alpha n/t_{99}$, where t_{99} represents the time to 99% consolidation. The conventional consolidation theory defines $t_{99} = T_{99}H^2/c_v$, where c_v is the consolidation coefficient; H is the drainage path length; and the time factor $T_{99} \approx 3$ (e.g. Lambe & Whitman, 1969).

The approach is illustrated through consolidation analyses of two NC clay specimens with thicknesses, $H = 2$ cm and 20 cm. The 2 cm and 20 cm thick specimens with $c_v = 10^{-3}$ (cm^2/s) reach 99% consolidation at $t_{99} \approx 3{\cdot}33$ h ($\approx 1{\cdot}2 \times 10^4$ s), and 333 h ($\approx 1{\cdot}2 \times 10^6$ s), respectively. Assuming $\rho_\alpha = 0{\cdot}009$ and porosity, $n = 0{\cdot}70$, the average creep rates for the 2 cm and 20 cm thick specimens are $R_{a0} = 0{\cdot}18$%/h ($=5 \times 10^{-7}$/s) and $0{\cdot}18 \times 10^{-2}$%/h ($=5 \times 10^{-9}$/s), respectively. The analyses use a finite-difference model to simulate the IL consolidation test, with initial creep rates assigned to all nodes across the height of the specimens. Fig. 7 illustrates the influence of the assumed initial creep rates (R_{a0}) on the pore pressure response evaluated at the base of the two specimens. The results show qualitatively similar behaviour for both specimens, with monotonic decreases in the base pore pressure. In contrast, if both specimens have the same initial creep rate ($R_{a0} = 0{\cdot}18$%/h), then there is an unexpected rise in base pore pressure for the 20 cm thick specimen, similar to predictions of most existing isotache models (Yuan & Whittle, 2013). This distinct pore pressure response becomes more pronounced when extrapolating to field scale where the typical creep rate of a 10 m thick NC clay layer is six orders of magnitude smaller than the one at laboratory scale. In this respect, a rational estimation of creep rate in the proposed model is essential for reliable predictions of long-term consolidation at field scale.

Description of full spectrum thickness effects

A second important feature of the proposed formulation is the ability to represent diverse observations of primary consolidation for clay layers of different thicknesses, between the limiting behaviours corresponding to hypotheses A and B (Ladd *et al.*, 1977). Figs 8(a)–8(d) illustrate typical model predictions of consolidation response under incremental loading for layers with $H = 2$ cm and 20 cm. Fig. 8(a) shows the depth averaged relation of void ratio, e, plotted against effective stress, σ'_v, for a reference material with the rate-dependency parameter, $\beta = \rho_\alpha/\rho_c$. The model predicts larger strains at the EOP for the thicker clay layer. As expected, the corresponding results for average void ratio plotted against elapsed time, Fig. 8(b), conform to hypothesis B and both specimens converge to a unique secondary compression line in log$e$–log$t$ space.

Figure 8(c) shows the corresponding model simulations for the case with $\beta = 0$. The two clay layers ($H = 2$ and 20 cm) exhibit a unique log$e$–log σ'_v curve. However, this result differs from rate-independent behaviour in the following aspects: (*a*) an elastoplastic model will predict a stress–void ratio relation that conforms to the input LCC line, whereas the proposed model with $\beta = 0$ predicts a curved compression path in log$e$–log σ'_v space, which reflects the intrinsic viscous characteristics of clay compression behaviour; (*b*) the proposed model with $\beta = 0$ allows concurrent creep during consolidation and secondary compression after EOP for both specimens. Fig. 8(d) shows that the time evolution of the average void ratio of the thicker specimen can be obtained by a linear transformation of the time scale (i.e. the two specimens have unique behaviour when plotted in log$e$–log (t/H^2) space). This behaviour corresponds to hypothesis A behaviour.

In summary, by varying the rate-sensitivity parameter β from ρ_α/ρ_c to 0, the proposed model can represent both

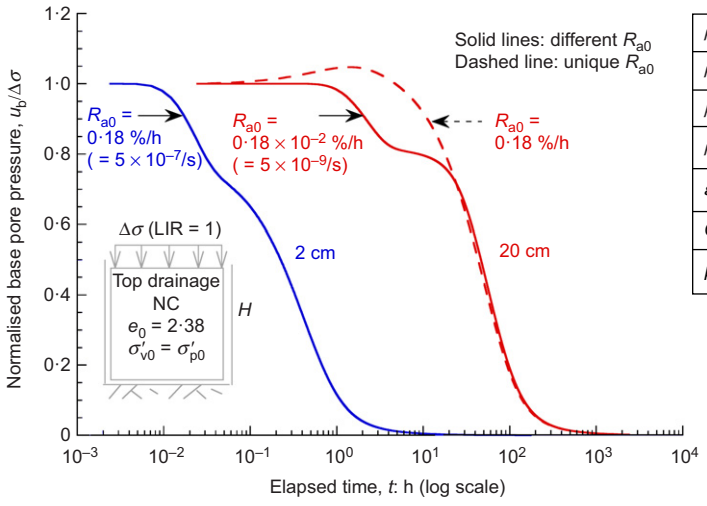

ρ_c	0·191
ρ_r	0·019
β	0·047
ρ_α/ρ_c	0·047
$\dot{\varepsilon}_{ref}$: %/h	$3{\cdot}6 \times 10^{-2}$
C_k	0·78
k_0: cm/s	$7{\cdot}38 \times 10^{-8}$

Fig. 7. Influence of R_{a0} on the predicted responses of base pore pressure for 2 cm and 20 cm thick specimens of NC clay

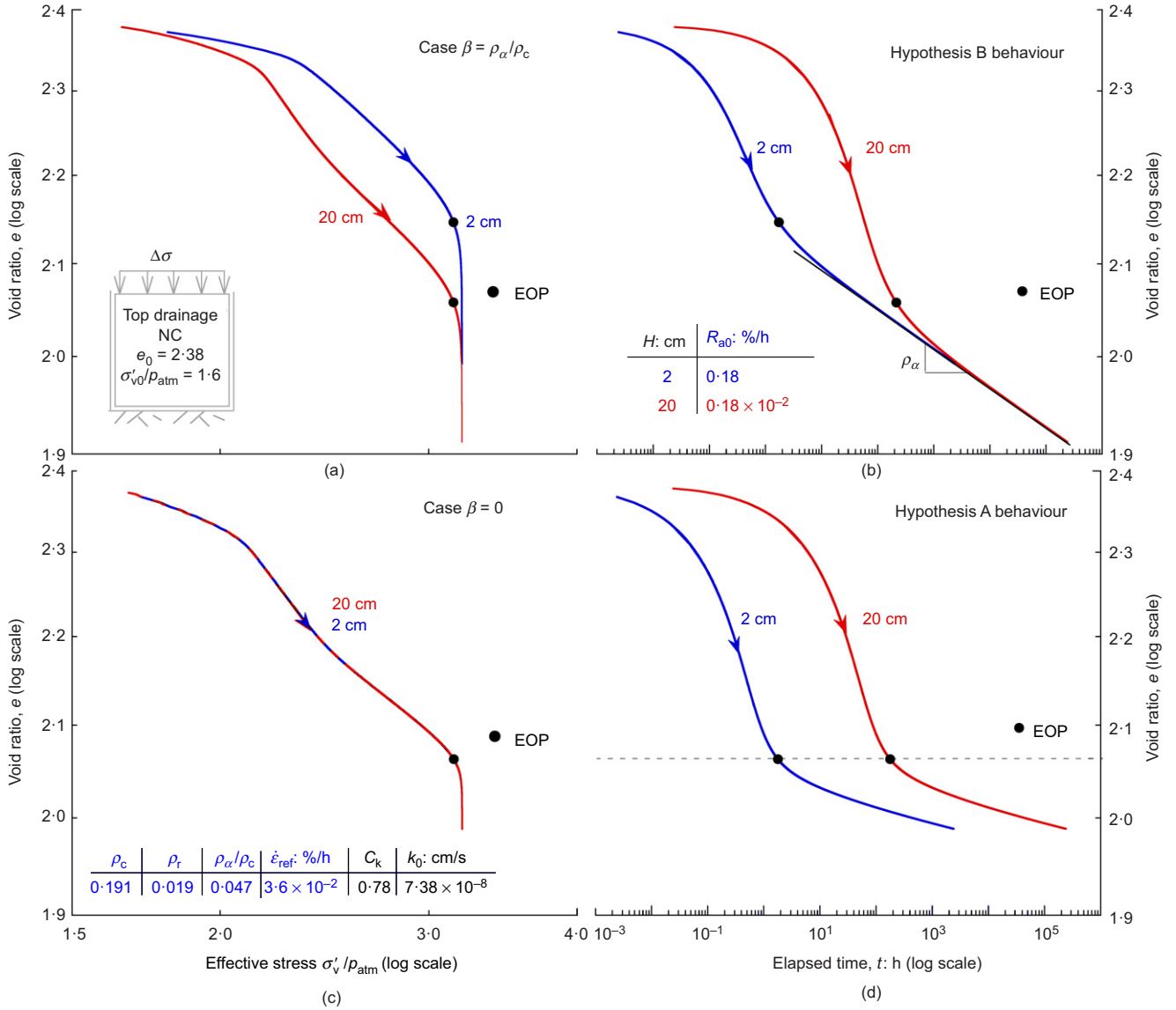

Fig. 8. Illustration of model predictions of IL consolidation behaviour for 2 cm and 20 cm thick specimens of NC clay: (a) effective stress–void ratio with $\beta = \rho_\alpha/\rho_c$; (b) void ratio–elapsed time with $\beta = \rho_\alpha/\rho_c$; (c) effective stress–void ratio with $\beta = 0$; (d) void ratio–elapsed time with $\beta = 0$

hypotheses A and B behaviour. Hence, it provides a unified formulation that can cover a full spectrum of thickness effects on consolidation behaviour.

INTERPRETATION OF DATA FOR OSAKA BAY MUD

This section illustrates the application of the proposed model for interpreting the thickness effects of IL consolidation on specimens of Osaka Bay mud (OBM) unit Ma11, a high-plasticity, Pleistocene clay with $w_L = 85{\cdot}9\%$ and $I_P = 60{\cdot}3\%$. Watabe *et al.* (2008) report data from experiments with oedometer test cells connected hydraulically in series. This configuration enables comparisons for a range of drainage path lengths while minimising the wall friction between the specimen and the consolidation ring. The test specimens in each oedometer cell are independently consolidated to the in situ stress level, $\sigma'_{v0} = 489$ kPa (corresponding to an OCR = 1·43) using standard IL procedures with 24 h load intervals. They are then connected in series and loaded to a final consolidation stress level of 1080 kPa for about 20 days.

Figure 9(a) plots the depth-averaged compression strain, ε, against logarithm of the elapsed time, t, for OBM specimens with drainage path lengths, $H = 2$ cm, 5 cm, 10 cm and 20 cm. The 5 cm, 10 cm and 20 cm thick specimens show similar strain levels at EOP (i.e. hypothesis A), whereas the thinnest specimen ($H = 2$ cm) exhibits a much smaller strain at EOP (consistent with hypothesis B). These discrepancies in the consolidation behaviour of OBM specimens with different thicknesses have been previously attributed to heterogeneities among the intact samples of OBM (Watabe *et al.*, 2008); a quantitative explanation is still lacking.

Model interpretation

The proposed model is implemented in finite-difference analyses to simulate consolidation behaviour of OBM. These simulations assume an initial internal strain rate, $R_{a0} = 5{\cdot}8 \times 10^{-3}$%/h across the depth to reproduce the average creep rate, $4{\cdot}2 \times 10^{-3}$%/h, measured at σ'_{v0} prior to the main consolidation stage. Two sets of β values: (*a*) $\beta = 0$ and (*b*) $\beta = \rho_\alpha/\rho_c$ are then used to reproduce the IL consolidation behaviour of OBM specimens.

For the first set of simulations with $\beta = 0$, data for the 5 cm thick specimen are used as a reference for model

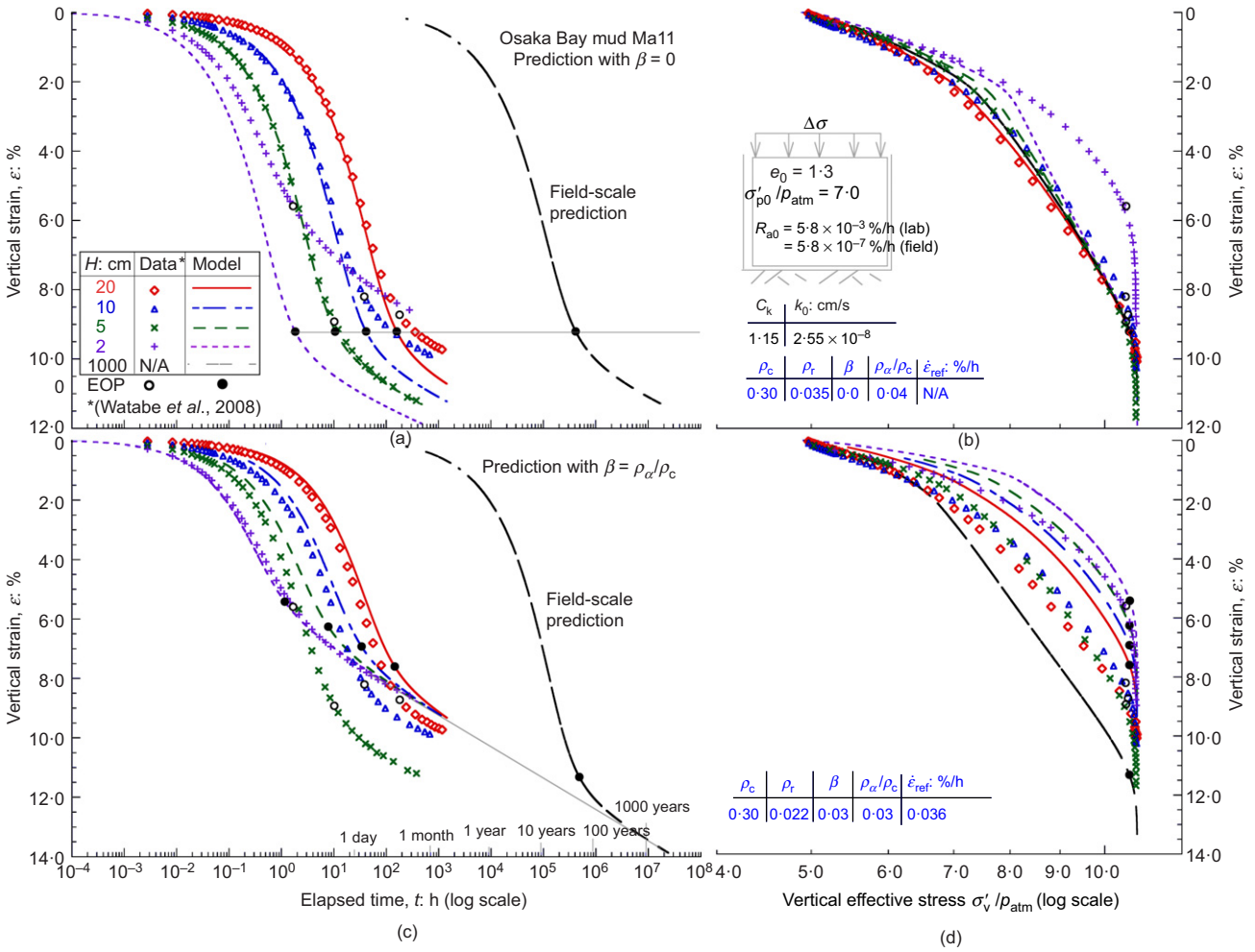

Fig. 9. Comparison of experimental results and model predictions for IL consolidation of lightly OC OBM (unit Ma11): (a) compression–elapsed time with $\beta = 0$; (b) effective stress–strain with $\beta = 0$; (c) compression–elapsed time with $\beta = \rho_\alpha/\rho_c$; (d) effective stress–strain with $\beta = \rho_\alpha/\rho_c$

calibration. The compressibility parameters, $\rho_c = 0{\cdot}35$ and $\rho_r = 0{\cdot}035$, are determined to fit the strain plotted against logarithm of effective stress, ε–log σ'_v curve for 5 cm thick specimen (Fig. 9(b)). They are consistent with the range of $\rho_c = 0{\cdot}27 \sim 0{\cdot}35$ and $\rho_r = 0{\cdot}022 \sim 0{\cdot}035$ determined from prior data of CRS and conventional IL oedometer tests for OBM unit Ma11 (Akai & Tanaka, 1999; Jeon, 2012). The parameter ρ_α is calibrated by fitting the corresponding secondary compression curve, with a best-fit value of $\rho_\alpha/\rho_c = 0{\cdot}04$. There is no need to determine the reference strain rate, $\dot{\varepsilon}_{ref}$.

Figure 9(a) compares the predicted ε–log$t$ curves with the experimental results for specimens with different thicknesses. Owing to the heterogeneity of initial void ratio among the samples in the interconnected oedometer cells, the authors only seek to describe the experimental results in an averaged sense by averaging compression strain and effective stress across the whole specimen. The results show the following.

(*a*) All specimens share the same strain at EOP, as expected for hypothesis A.
(*b*) The model predictions are generally consistent with the experimental measurements for 5 cm, 10 cm and 20 cm thick specimens, but clearly deviate from the behaviour of the 2 cm thick specimen.

Figure 9(b) plots the corresponding ε–log σ'_v curves for all specimens. As can be seen, all the predicted curves concentrate in a narrow band and converge to a unique EOP state. The predictions for the thicker specimens (5 cm, 10 cm and 20 cm) closely correspond to the experimental results. However, the prediction noticeably underestimates the measured increase in effective stress, σ'_v, at a given strain, ε, for the 2 cm thick specimen.

For the second set of simulations with $\beta = \rho_\alpha/\rho_c$, data for the 2 cm thick specimen are used to calibrate the model. The compression parameters, $\rho_c = 0{\cdot}30$ and $\rho_r = 0{\cdot}022$, are selected to match the ε–log σ'_v curve for the 2 cm thick specimen (Fig. 9(d)) and still within the range obtained from prior data. The ratio of $\rho_\alpha/\rho_c = 0{\cdot}03$ is selected to achieve the best fit to the measured secondary compression behaviour in ε–log$t$ space, as shown in Fig. 9(c). The reference strain rate, $\dot{\varepsilon}_{ref} = 3{\cdot}6 \times 10^{-2}$%/h, corresponds to the 24 h strain rate in IL oedometer tests. Fig. 9(c) compares the predictions of ε–log$t$ curves with experimental data for all specimens. The results show the following.

(*a*) The proposed model with $\beta = \rho_\alpha/\rho_c$ clearly predicts hypothesis B behaviour. The resulting strain at EOP increases with the specimen thickness, and the secondary compression behaviour converges to a unified, linearised ε–log$t$ relation.
(*b*) The prediction matches closely the measured behaviour for the 2 cm thick specimen, but significantly deviates from the results of thicker specimens (5 cm, 10 cm and 20 cm). The model underestimates the EOP strain by 40% for 5 cm thick specimen, and by 18% and 15% for 10 cm and 20 cm thick specimens, respectively.

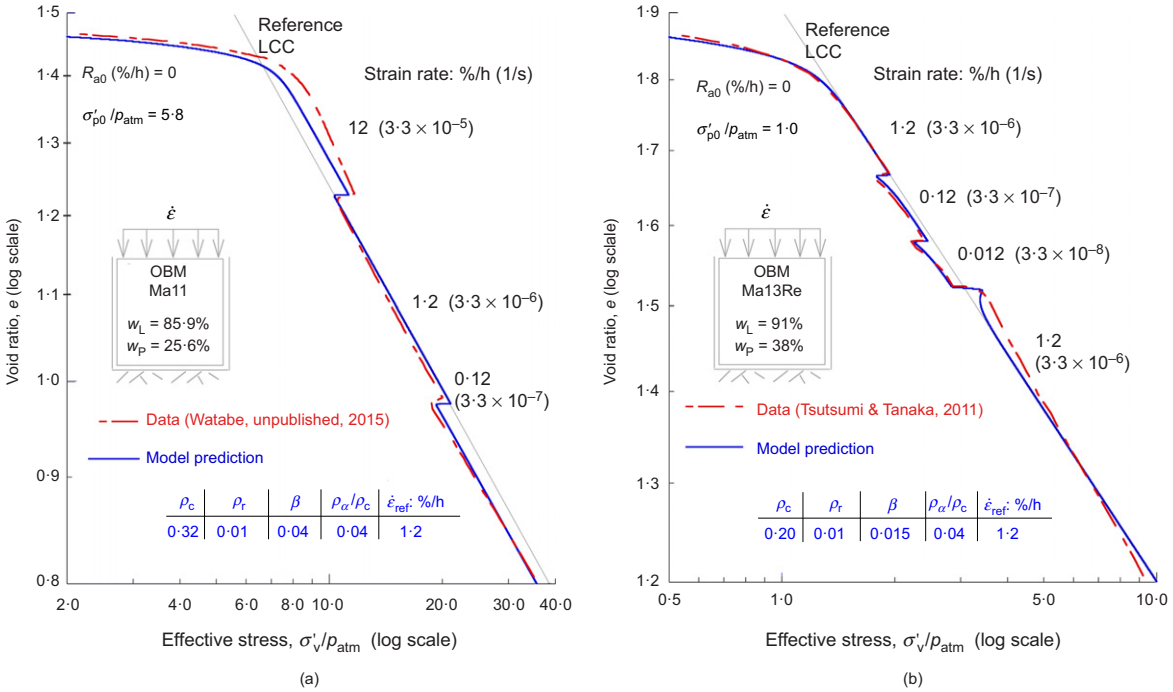

Fig. 10. Interpretation of CRS tests with step-changed strain rates on OBM: (a) isotache behaviour for Ma11 sample; (b) temporary strain rate effects for reconstituted Ma13Re sample

Figure 9(d) compares the numerical predictions of ε–log σ'_v curves with the experimental results. As can be seen, the predictions show thickness-dependent EOP states, and thinner specimens generate less strain at EOP (indicating higher stress resistance against deformation at the same strain level). These characteristics are qualitatively consistent with the experimental data.

Implications from CRS data

The proposed formulation infers an inherent link between the thickness effects in IL consolidation and the rate effects in the CRS test, by way of the rate-sensitivity parameter β. In this respect, data from CRS tests on OBM are closely examined to justify the discrepancy in the parameter β from the above interpretation of IL oedometer tests as follows.

Figure 10(a) shows the void ratio, e, plotted against effective stress, σ'_v, relation of a CRS test on OBM unit Ma11 (Watabe, unpublished data, 2015), where the applied strain rate reduces from 12%/h to 0·12%/h in three steps. Parallel shifts in the compression curve are observed upon step-wise changes in strain rates, which appear to be consistent with isotache characteristics. As shown in Fig. 10(a), the prediction using the proposed model with $\beta = \rho_\alpha/\rho_c = 0{\cdot}04$ fits these data very closely.

In contrast, Fig. 10(b) presents CRS test data reported by Tsutsumi & Tanaka (2011) on a specimen of reconstituted OBM (unit Ma13Re; $w_L = 91\%$; $I_P = 53\%$), where strain rates are stepped between 1·2%/h and 0·012%/h (i.e. ten times slower than those used in prior tests for the intact Ma11 specimen). This change in strain rate does not produce parallel shifts in log$e$–log σ'_v curves, as the induced changes in effective stress show a transient response. Fig. 10(b) illustrates that the proposed model with $\beta = 0{\cdot}015 < \rho_\alpha/\rho_c = 0{\cdot}04$, closely captures these transient characteristics.

Figure 11 relates these CRS tests to the prior interconnected oedometer tests by comparing the relative magnitude of the representative strain rates for these experiments.

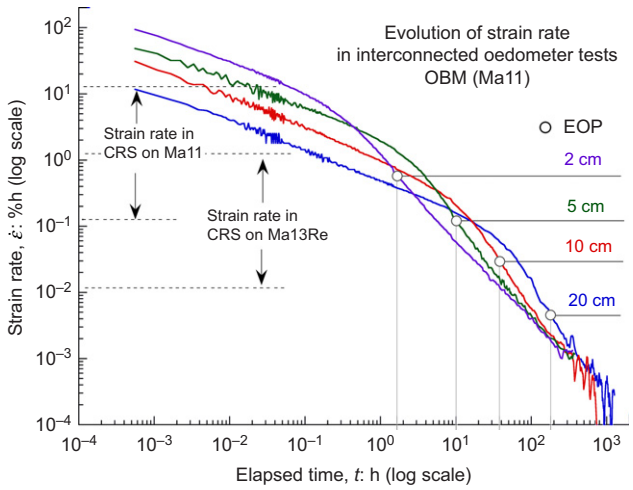

Fig. 11. Comparison of relative strain rates between CRS tests with step-changed strain rates and interconnected oedometer tests on OBM (interpreted from Watabe *et al.*, 2008; Tsutsumi & Tanaka, 2011)

This comparison leads to new perspectives on explaining the contradictory thickness effects for OBM as follows.

(*a*) Figure 11 shows that the 2 cm thick specimen in the IL oedometer test consolidates at relatively high strain rates (0·1∼1·0%/h), which are in the range of strain rate for the CRS test in Fig. 10(a). Over this range, the isotache characteristics observed in CRS test verify the prior selection of $\beta = \rho_\alpha/\rho_c$ for representing hypothesis B behaviour in the IL oedometer test.

(*b*) The 5 cm, 10 cm and 20 cm thick specimens undergo slower consolidation with EOP strain rates in the range between 1×10^{-1} and 10^{-3}%/h, which is comparable with the range of strain rate for CRS data in Fig. 10(b). The strain rate over this range shows temporary influence on the behaviour of CRS test, which implies

a smaller value of parameter β (i.e. $\beta < \rho_\alpha/\rho_c$). This verifies the trend of selecting $\beta = 0$ for describing the hypothesis A behaviour of thicker specimens in IL consolidation tests and may be of more direct relevance for consolidation at field scale.

Field-scale prediction

The proposed model with parameters determined from prior interconnected oedometer data is then applied to predict the consolidation behaviour of OBM unit Ma11 layer at the site of Kansai International Airport – Island II. According to the sub-seabed soil profile (Mesri & Funk, 2015), the Ma11 Pleistocene layer, approximately 70 m below the seabed, consists of upper and lower units with a total thickness of 20 m and allows possible drainage through top and bottom sand layers. The construction of Island II began in 1999 and was completed in 2007 with maximum recorded reclamation loads on the seabed ranging from 500 to 600 kPa.

The simulation simplifies the field conditions and assumes a 10 m thick OBM layer with one-way drainage on top consolidates at an averaged in situ effective stress of 489 kPa and OCR = 1·43 subjected to a step loading of 590 kPa (i.e. the same load step as the interconnected oedometer tests). The initial internal strain rate was set as $R_{a0} = 5{\cdot}8 \times 10^{-7}$%/h for a 10 m thick layer, which is four orders of magnitude smaller than the prior value for laboratory specimens (ranging in thickness from 2 to 20 cm, where $R_{a0} = 5{\cdot}8 \times 10^{-3}$%/h).

The field-scale simulations use two sets of parameters. The first uses $\beta = 0$ and parameters determined from the data of a 5 cm specimen. Fig. 9(a) shows that the predicted ε–log$t$ curve for a 10 m thick layer produces the same EOP strain as those for laboratory specimens; and the former can be achieved by transforming the latter in time scale. The predicted ε–log σ'_v curve also matches closely the predictions at laboratory scale, as shown in Fig. 9(b). These observations are consistent with hypothesis A. The second simulation uses $\beta = \rho_\alpha/\rho_c$ and parameters determined from the data of a 2 cm thick specimen. In this case, the 10 m thick layer shows much larger strain than the laboratory specimens throughout consolidation, as shown in Figs 9(c) and 9(d). The ε–log$t$ curves predicted for all thickness scales eventually converge to a unified secondary compression behaviour. These results agree with hypothesis B.

Figure 12 plots the vertical compression strain against time (expressed in terms of date after construction) from the two field-scale simulations. It is assumed that the fill was applied as a step load in 2003 (an approximation to the ramped period of land reclamation, 1999–2007). The data of vertical compression in Ma11 layer are readily estimated from the difference in settlement measured at top and bottom of Ma11 layer, with magnetic differential settlement gauges at monitor points 1 and 2 at Island II site (MP1-II and MP2-II; Funk, 2013). Fig. 12 shows that predictions obtained with two sets of parameters (and simplified assumptions on boundary conditions) generally match the measured data. As the data are only available from 2002 to 2011, the measurement for only 10 years is too limited to indicate which set of parameters will lead to better prediction of long-term settlements.

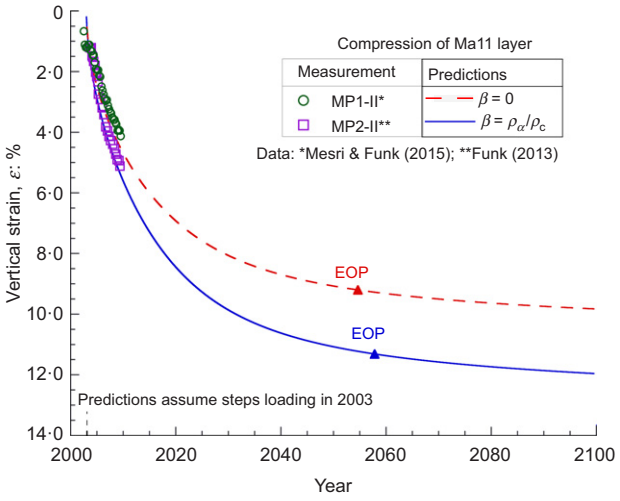

Fig. 12. Comparison of model predictions and measurements for the time history of compression in OBM (unit Ma11) layer

CONCLUSIONS

This paper presents a new EVP formulation for describing the general 1D compression behaviour of clays. The proposed model combines the bilinear log$e$–log σ'_v framework (Pestana, 1994), with a rate-dependent constitutive relation. The key component is a novel evolution law, which attributes the macro-scale viscoplastic strain rate, $\dot{\varepsilon}^{vp}$, to an internal state variable, R_a, representing the perturbation of clay particles due to the prior strain rate history.

The model introduces five material parameters and two internal state variables. Among these, the key parameter is the rate-sensitivity, β, which can characterise a wide range of rate-dependent behaviour, including isotache-type behaviour ($\beta = \rho_\alpha/\rho_c$) (Suklje, 1957) and temporary strain rate effects ($\beta = 0$) (Tatsuoka *et al.*, 2002) under CRS loading conditions. The viscous property ρ_α controls secondary compression behaviour and the effective stress response under relaxation. All the material parameters can be experimentally calibrated using data for CRS tests and IL oedometer tests. The difficulties in estimating the initial internal strain rate, R_{a0}, can be resolved by giving a realistic estimation of the strain rate from prior consolidation.

The performance and the advantages of the proposed model have been demonstrated through several benchmarks and can be summarised as listed below.

(*a*) The model allows a rational estimate of initial creep rates when predicting IL consolidation behaviour, and hence overcomes the drawbacks of existing isotache frameworks, which tend to overestimate the initial creep rate for larger specimens.
(*b*) By using $\beta = 0$ and ρ_α/ρ_c the proposed constitutive model predicts hypothesis A and B behaviour, respectively, and hence provides a unified framework for a wide range of thickness effects of IL consolidation.
(*c*) A series of consolidation tests on OBM, unit Ma11, show apparently contradictory consolidation behaviour. Using the proposed model it is confirmed that differences in the rate parameter β are needed to explain these data and show that β may vary with the strain rates used in the laboratory tests. This inference provides new insight to explaining discrepancies in the reported compression behaviour of OBM.
(*d*) The proposed model facilitates versatile predictions of long-term consolidation of OBM at Kansai International Airport site. The field data for only 10 years are limited to justify which set of parameters leads to more realistic predictions of long-term settlement.

This paper has focused on the development and application of the proposed model for the 1D consolidation behaviour of

clay. The framework has also been generalised for three-dimensional constitutive relations to describe clay behaviour under complex loading conditions (MIT-SR; Yuan, 2016) and integrated within finite-element software (Sottile, 2016).

ACKNOWLEDGEMENTS

This research was supported in part by Ferrovial-Agroman through the MIT-Ferrovial programme and by the MIT–Singapore Alliance for Research and Technology (SMART). The authors are particularly grateful for the generous assistance and encouragement from Dr Yoichi Watabe (PARI, Japan) and for advice on soil behaviour from their colleagues Professor Jack Germaine and the late Professor Charles C. Ladd.

NOTATION

C_c	virgin compression index
C_k	variation in (log) hydraulic conductivity with void ratio
C_α	secondary compression coefficient
c_v	vertical consolidation coefficient
e	void ratio
H	thickness or drainage length of clay layer
I_P	plasticity index
k	hydraulic conductivity
M	one-dimensional modulus
m_t	transient coefficient
n	porosity
R_a	internal strain rate
T_{99}	normalised time factor for 99% consolidation
t	elapsed time
t_{99}	time to achieve 99% consolidation
w_L	liquid limit
α	rate-sensitivity of isotache power-law formulation
β	rate-sensitivity parameter of steady state of R_a
ε	vertical strain (compression positive)
$\dot{\varepsilon}$	total strain rate
$\dot{\varepsilon}^e$	elastic strain rate
$\dot{\varepsilon}^{vp}$	viscoplastic strain rate
$\dot{\varepsilon}_{ref}$	reference strain rate
ρ_c	compressibility over limiting compression curve pressure range
ρ_r	compressibility over reloading range
ρ_α	creep coefficient (proposed model)
σ'_v	vertical effective stress
σ'_p	stress state variable

REFERENCES

Akai, K. & Tanaka, Y. (1999). Settlement behavior of an off-shore airport KIA. In *Geotechnical engineering for transportation infrastructure: theory and practice, planning and design, construction and maintenance: proceedings of the 12th European conference on soil mechanics and geotechnical engineering* (eds F. B. J. Barends, J. Lindenberg, H. J. Luer, A. Verruijt and L. de Quelerij), pp. 1041–1046. Boca Raton, FL, USA: CRC Press.

Bjerrum, L. (1967). Engineering geology of Norwegian normally-consolidated marine clays as related to settlements of buildings. *Géotechnique* **17**, No. 2, 83–118, https://doi.org/10.1680/geot.1967.17.2.83.

Bodas Freitas, T. M., Potts, D. M. & Zdravkovic, L. (2011). A time dependent constitutive model for soils with isotach viscosity. *Comput. Geotech.* **38**, No. 6, 809–820.

Buisman, A. (1936). Results of long duration settlement tests. *Proceedings of the 1st international conference on soil mechanics and foundation engineering*, vol. 1, pp. 103–107. Cambridge, MA, USA: Harvard University.

Butterfield, R. (1979). A natural compression law for soils (an advance on *e*–log*p*′). *Géotechnique* **29**, No. 3, 469–480, https://doi.org/10.1680/geot.1979.29.4.469.

Degago, S. & Grimstad, G. (2014). Significance of sample quality in settlement analysis of field cases. In *Proceedings of numerical methods in geotechnical engineering (NUMGE 2014)* (eds M. A. Hicks, R. B. J. Brinkgreve and A. Rohe), pp. 153–158. Boca Raton, FL, USA: CRC Press.

Den Haan, E. J. (1996). A compression model for non-brittle soft clays and peat. *Géotechnique* **46**, No. 1, 1–16, https://doi.org/10.1680/geot.1996.46.1.1.

Feng, T. W. (1991). *Compressibility and permeability of natural soft clays and surcharging to reduce settlements*. PhD thesis, University of Illinois at Urbana–Champaign, Champaign, IL, USA.

Funk, J. R. (2013). *Settlement of the Kansai international airport islands*. PhD thesis, University of Illinois at Urbana–Champaign, Champaign, IL, USA.

Garlanger, J. E. (1972). The consolidation of soils exhibiting creep under constant effective stress. *Géotechnique* **22**, No. 1, 71–78, https://doi.org/10.1680/geot.1972.22.1.71.

Imai, G. (1995). Analytical examinations of the foundations to formulate consolidation phenomena with inherent time-dependence. Keynote lecture. In *Compression and consolidation of clayey soils, IS-Hiroshima* (eds O. Kusakabe and H. Yoshikuni), vol. 2, pp. 891–935. Rotterdam, the Netherlands: Balkema.

Jamiolkowski, M., Ladd, C. C., Germaine, J. T. & Lancellotta, R. (1985). New developments in field and laboratory testing of soils. In *Proceedings of the 11th international conference on soil mechanics and foundation engineering*, vol. 1, pp. 57–153. Rotterdam, the Netherlands: Balkema.

Janbu, N. (1963). Soil compressibility as determined by oedometer and triaxial tests. *Proceedings of the 3rd European conference soil mechanics*, Wiesbaden, Germany, vol. 1, pp. 19–25.

Jeon, B. G. (2012). *Numerical assessment for long-term behavior of the Pleistocene marine foundations due to construction of large-scale offshore airport fill*. PhD thesis, Kyoto University, Kyoto, Japan.

Jiang, Y. M. & Liu, M. (2009). Granular solid hydrodynamic. *Granular Matter* **11**, No. 3, 139–156.

Jiang, Y. M. & Liu, M. (2013). Stress and rate-controlled granular rheology. *AIP Conference Proc.* **1542**, 52–59.

Juarez-Badillo, E. (1965). Compressibility of soils. In *Proceedings of the 5th symposium of the Civil and Hydraulic Engineering Department on behavior of soils under stress*, vol. 1, A2, pp. 1–35. Bangalore, India: Indian Institute of Science.

Kim, Y. T. & Leroueil, S. (2001). Modeling the viscoplastic behavior of clays during consolidation: application to Berthierville clay in both laboratory and field conditions. *Can. Geotech. J.* **38**, No. 3, 484–497.

Korchaiyapruk, A. (2007). *Experimental and numerical study of primary consolidation of soft clay*. PhD thesis, Massachusetts Institute of Technology, Cambridge, MA, USA.

Ladd, C. C., Foott, R., Ishihara, K., Schlosser, F. & Poulos, H. G. (1977). Stress–deformation and strength characteristics. In *Proceedings of the 9th international conference on soil mechanics and foundation engineering*, pp. 421–494. Tokyo, Japan: Japanese Society of Soil Mechanics and Foundation Engineering.

Lambe, T. W. & Whitman, R. V. (1969). *Soil mechanics*. New York, NY, USA: Wiley.

Le, T. M., Fatahi, B. & Khabbaz, H. (2012). Viscous behavior of soft clay and inducing factors. *Geotech. Geol. Engng* **30**, No. 5, 1069–1083.

Leroueil, S., Kabbaj, M., Tavenas, F. & Bouchard, R. (1985). Stress–strain–strain rate relation for the compressibility of sensitive natural clays. *Géotechnique* **35**, No. 2, 159–180, https://doi.org/10.1680/geot.1985.35.2.159.

Mesri, G. & Castro, A. (1987). C_a/C_c concept and K_0 during secondary compression. *ASCE J. Geotech. Engng* **113**, No. 3, 230–247.

Mesri, G. & Choi, Y. K. (1985a). The uniqueness of the end-of-primary (EOP) void ratio-effective stress relationship. In *Proceedings of the 11th international conference on soil mechanics and foundation engineering*, vol. 2, pp. 587–590. Rotterdam, the Netherlands: Balkema.

Mesri, G. & Choi, Y. K. (1985b). Settlement analysis of embankments on soft clays. *ASCE J. Geotech. Engng* **1**, No. 4, 441–464.

Mesri, G. & Funk, J. R. (2015). Settlement of the Kansai international airport islands. *J. Geotech. Geoenviron. Engng* **141**, No. 2, 1–16.

Perzyna, P. (1966). Fundamental problems in viscoplasticity. *Adv. Appl. Mech.* **9**, 243–377.

Pestana, J. M. (1994). *A unified constitutive model for clays and sands*. PhD thesis, Massachusetts Institute of Technology, Cambridge, MA, USA.

Pestana, J. M. & Whittle, A. J. (1999). Formulation of a unified constitutive model for clays and sands. *Int. J. Numer. Analyt. Methods Geomech.* **23**, No. 12, 1215–1243.

Schofield, A. & Wroth, P. (1968). *Critical state soil mechanics*. New York, NY, USA: McGraw-Hill.

Shattuck, M. D., Ingale, R. A. & Reis, P. M. (2009). Granular thermodynamics. In *Proceedings of the 6th international conference on micromechanics of granular media: powders and grains*, vol. 1145, pp. 43–50. Melville, NY, USA: AIP Publishing.

Smith, D. W. (2001). Granular temperature. *Int. J. Geomech.* **1**, No. 2, 249–271.

Sottile, M. (2016). *Implementation and evaluation of a recently developed rate-dependent effective stress soil model, MIT-SR*. SM thesis, Massachusetts Institute of Technology, Cambridge, MA, USA.

Suklje, L. (1957). The analysis of the consolidation process by the isotaches method. In *Proceedings of the 4th international conference on soil mechanics and foundation engineering*, pp. 201–206. London, UK: Butterworths Scientific.

Tatsuoka, F., Ishihara, M., Di Benedetto, H. & Kuwano, R. (2002). Time-dependent shear deformation characteristics of geomaterials and their simulation. *Soils Found.* **42**, No. 2, 103–129.

Taylor, D. W. (1942). *Research on consolidation of clays*, Report Serial 82. Cambridge, MA, USA: Department of Civil Engineering, Massachusetts Institute of Technology.

Terzaghi, K. (1943). *Theoretical soil mechanics*. New York, NY, USA: John Wiley and Sons.

Terzaghi, K. & Peck, R. B. (1948). *Soil mechanics in engineering practice*, 1st edn. New York, NY, USA: John Wiley and Sons.

Tsutsumi, A. & Tanaka, H. (2011). Compressive behavior during the transition of strain rates. *Soils Found.* **51**, No. 5, 813–822.

Vermeer, P. A. & Neher, H. P. (1999). A soft soil model that accounts for creep. In *Beyond 2000 in computational geotechnics: 10 years of PLAXIS International*, pp. 249–262. Rotterdam, the Netherlands: Balkema.

Watabe, Y., Udaka, K., Kobayashi, M., Tabata, T. & Emura, T. (2008). Effects of friction and thickness on long-term consolidation behavior of Osaka Bay clays. *Soils Found.* **48**, No. 4, 547–561.

Watabe, Y., Udaka, K., Nakatani, Y. & Leroueil, S. (2012). Long-term consolidation behavior interpreted with isotache concept for worldwide clays. *Soils Found.* **52**, No. 3, 449–464.

Yin, J. H. & Graham, J. (1994). Equivalent times and one-dimensional elastic viscoplastic modelling of time-dependent stress-strain behavior of clays. *Can. Geotech. J.* **31**, No. 1, 42–52.

Yin, Z. Y., Chang, C. S., Karstunen, M. & Hicher, P. V. (2010). An anisotropic elastic-viscoplastic model for soft clays. *Int. J. Solids Structs* **47**, No. 5, 665–677.

Yin, Z. Y., Zhu, Q. Y., Yin, J. H. & Ni, Q. (2014). Stress relaxation coefficient and formulation for soft soils. *Géotechnique Lett.* **4**, No. 1, 45–51, https://doi.org/10.1680/geolett.13.00070.

Yoshikuni, H., Kusakabe, O., Okada, M. & Tajima, S. (1995). Mechanism of one-dimensional consolidation. In *Compression and consolidation of clayey soils, IS-Hiroshima* (eds O. Kusakabe and H. Yoshikuni), vol. 1, pp. 497–504. Rotterdam, the Netherlands: Balkema.

Yuan, Y. (2016). *A new elasto-viscoplastic model for rate-dependent behavior of clays*. PhD thesis, Massachusetts Institute of Technology, Cambridge, MA, USA.

Yuan, Y. & Whittle, A. J. (2013). Examination on time-dependent soil models in one-dimensional consolidation. In *Proceedings of constitutive modeling of geomaterials*, Beijing, China (eds Q. Yang, J.-M. Zhang, H. Zheng and Y. Yao), pp. 159–166. Berlin, Germany: Springer.

Zhang, Z. C. & Cheng, X. H. (2014). Effective stress in saturated soil: a granular solid hydrodynamic approach. *Granular Matter* **16**, No. 5, 761–769.